crystals

MDPI

Article

# A Five-Coordinate Copper(II) Complex Constructed from Sterically Hindered 4-Chlorobenzoate and Benzimidazole: Synthesis, Crystal Structure, Hirschfeld Surface Analysis, DFT, Docking Studies and Antibacterial Activity

**Abiodun A. Ajibola [1,*], Fouzia Perveen [2], Kalsoom Jan [2], Ibikunle I. Anibijuwon [3], Solomon E. Shaibu [4], Lesław Sieroń [5] and Waldemar Maniukiewicz [5,*]**

1 Department of Chemical Sciences, Crown-Hill University, P.M.B. 1605, Eiyenkorin, Ilorin 240213, Kwara State, Nigeria
2 Research Center for Modeling and Simulations (RCMS), NUST, H-12 Campus Islamabad, Islamabad 44000, Pakistan; fouzia_qau81@yahoo.com (F.P.); kal.j225@gmail.com (K.J.)
3 Department of Microbiology, Faculty Life sciences, University of Ilorin, P.M.B 1515, Ilorin 240213, Kwara State, Nigeria; kunledoexploit@gmail.com
4 Department of Chemistry, University of Uyo, P.M.B 1017, Uyo 520003, Akwa Ibom State, Nigeria; shaibusolomon@uniuyo.edu.ng
5 Institute of General and Ecological Chemistry, Lodz University of Technology, 116 Zeromskiego, 90-924 Lodz, Poland; leslaw.sieron@p.lodz.pl
* Correspondence: abiodunaajibola@gmail.com (A.A.A.); waldemar.maniukiewicz@p.lodz.pl (W.M.)

Received: 6 October 2020; Accepted: 21 October 2020; Published: 31 October 2020


**Abstract:** A new $Cu^{II}$ complex (**1**) was synthesized by reacting 4-chlorobenzoic acid, benzimidazole and metal salt using ethanol–water (1:1 v/v) as a solvent at room temperature. The complex was characterized by single-crystal X-ray analysis, FTIR and UV—vis spectroscopy. A distorted square pyramidal geometry of the $Cu^{II}$ center was observed from the single-crystal X-ray study, which also revealed that the uncoordinated oxygen atom of the carboxylate anions forms intermolecular hydrogen bonds with the N–H groups of the benzimidazole ligands. The Hirschfeld analysis results revealed that the molecular packing of **1** is mainly controlled by O . . . H (12.7%), Cl..H (16.4%), C...H (24.4%) and H...H (31.1%) contacts. Density functional theory (DFT) calculations were performed to compute the HOMO–LUMO energy gap and electrostatic potential map for the charge transfer regions within the molecule and identify the possible electrophilic and nucleophilic regions of the molecule. A number of reactivity parameters calculated on the basis of $E_{HOMO}$ and $E_{LUMO}$ show its significant polarizability and reactive nature. Complex **1** was also examined and screened for its potential antibacterial effect using the agar well diffusion method. The newly synthesized complex showed an effective and higher killing rate of the microbes in antibacterial testing compared to the parent ligand. The $Cu^{II}$ complex (**1**) showed an enhanced inhibitory activity against *P. aeruginosa* and equally demonstrated greater binding affinity with DNA gyrase (1KIJ) compared to its ligands according to the molecular docking studies.

**Keywords:** single-crystal X-ray diffraction; copper (II) complex; benzimidazole; DFT; molecular docking; antibacterial activity

## 1. Introduction

There have been numerous studies directed at the synthesis of new metal complexes with potential biological activity [1–6]. The use of transition metals with biologically active ligands yields new compounds with higher activity when compared with the metal ion or the coordinated ligands [7–10]. Benzimidazole (BZDH) is an N-containing heterocyclic compound that has been well documented over many years. Benzimidazole (BZDH) is known to be a monodentate ligand (Figure 1a) coordinating through the heterocyclic nitrogen atom [11]. A plethora of studies of benzimidazole and its derivatives have shown pharmacological activities [12–14]. Due to these properties, benzimidazole and its derivatives have been widely used until now as coligands with several metal ions in coordination chemistry [11,15–24]. The mode of coordination of nitrogenous donor ligands with other coligands, with respect to the metal center in the same system, can enhance the biological activity of metal complexes [24–26]. Metal ions such as copper have been studied and empirical evidence about their biological activity in many biochemical processes has been attained [27]. Copper ion is known to be one of the most widely studied metals in coordination chemistry because of its biological relevance and various applications [4]. Copper(II) carboxylate with pharmacological ligands is known to be more effective in combating and treating diseases compared to its parent ligands [9,28,29]. 4-Chlorobenzoic acid (4Clbz) bears one -COOH group (Figure 1b) that can fashion into monodentate, bidentate and multidentate modes of coordination [30–35]. According to the Cambridge Structural Database (CSD), and to the best of our knowledge, this is the first system that comprises 4-chlorobenzoic acid and benzimidazole with a copper center. In this paper, we aim for the synthesis, characterization, DFT calculation and antimicrobial activity of a new $Cu^{II}$ complex with 4-chlorobenzoate in the presence of benzimidazole. By using a molecular docking study, Cu(II) complex, 4-chlorobenzoic acid and benzimidazole were treated with DNA gyrase (1KIJ) to observe their various interactions and binding affinities.

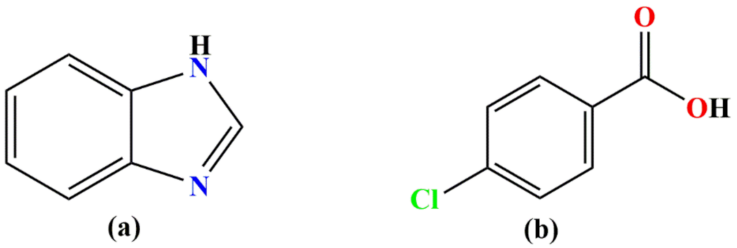


**Figure 1.** (**a**) Benzimidazole (BZDH); (**b**) 4-chlorobenzoic acid (4Clbz).

## 2. Experimental

### 2.1. Materials and Physical Measurements

All chemicals and solvents were reagent grade and were used as purchased commercially without any further purification. Fourier transform infrared spectra (FTIR) were recorded on SHIMADZU FTIR-8400S (Shimadzu Scientific Instruments, INC, USA). The UV—vis spectrum of the complex was recorded on a JENWAY 6405Uv/Vis spectrophotometer (Cole-Parmer Ltd., Stone, UK) using dimethyl sulfoxide (DMSO) as the solvent. The melting temperature of **1** was determined by the Digital Electrothermal Melting Point Apparatus model IA9100 (Cole-Parmer Ltd., Stone, UK).

### 2.2. Crystallographic Analysis

Single-crystal X-ray diffraction data were collected by the ω-scan technique using $MoK_\alpha$ ($\lambda$= 0.71073 Å) radiation. The title compound was studied at 100(3) K using a RIGAKU XtaLAB Synergy, Dualflex, Pilatus 300K diffractometer (Rigaku Corporation, Tokyo, Japan) [36] with a Photon Jet microfocus X-ray source. Data collection, cell refinement, data reduction and absorption correction were carried out using the CrysAlis PRO software [36]. The crystal structures were solved by using

direct methods with the SHELXT 2018/3 program [37]. Atomic scattering factors were taken from the International Tables for X-ray Crystallography. Positional parameters of non-H-atoms were refined by a full-matrix least-squares method on $F^2$ with anisotropic thermal parameters with the SHELXL 2018/3 program [38]. Hydrogen atoms participating in hydrogen bonding were found on the Fourier map and freely refined while the others were placed in calculated positions (C–H = 0.93–0.98 Å) and included as riding contributions with isotropic displacement parameters set to 1.2-times the $U_{eq}$ of the parent atom. Crystal data and structure refinement parameters are shown in Table 1.

**Table 1.** Crystal data and structure refinement parameters for **1**.

| Parameters | 1 |
|---|---|
| Empirical formula | $C_{28}H_{20}Cl_2CuN_4O_4$ |
| Formula weight | 610.93 |
| Temperature (K) | 100(3) |
| Wavelength (Å) | 0.71073 |
| Crystal system | Monoclinic |
| Space group | $P2_1/c$ |
| a (Å) | 14.5042(3) |
| b (Å) | 13.2293(2) |
| c (Å) | 13.6286(2) |
| α (°) | 90 |
| β (°) | 104.816(2) |
| γ(°) | 90 |
| Volume ($Å^3$) | 2528.12(8) |
| Z | 4 |
| Density ($Mg/m^3$) | 1.605 |
| Absorp. coeff. ($mm^{-1}$) | 1.120 |
| F(000) | 1244 |
| Crystal size ($mm^3$) | 0.35 × 0.25 × 0.15 |
| Theta range for data collection | 2.4, 25.0 |
| Index ranges | −1 7≤ h ≤ 17; −15 ≤ k ≤ 15; −16 ≤ l ≤ 16 |
| Reflection collected | 71647 |
| Independent reflections | 4469 [R(int) = 0.055] |
| Goodness of fit on $F^2$ | 1.13 |
| Final R indices [I > 2sigma(I)] | 0.0361 |
| R indices (all data) | 0.0427 |
| Largest diff. peak and hole ($eÅ^{-3}$) | 1.12 and −0.42 |

### *2.3. Hirschfeld Surface Analysis*

The Hirschfeld surfaces (HS) [39] and the related 2D-fingerprint plots (FP) [40] were calculated using Crystal Explorer software ver. 17.5 [41]. An in-depth introduction to HS analysis has been described elsewhere [42]. The crystal data imported from CIF files were used for analysis. Before starting the calculations, the bond lengths to hydrogen atoms were set to standardized neutron values (O–H = 0.983Å, N–H = 1.009 Å and C–H = 1.083 Å).

### *2.4. DFT Calculation*

Computational DFT studies were performed using the Gaussian 09 software [43]. Gauss View 05 was employed for the graphical visualization of output files, molecular orbitals and the potential energy surface (PES) [44]. Complex **1** was optimized by the hybrid B3LYP method with a 6-311G(d,p) basis set. Recently, the B3LYP method has gained popularity with great reliability for the structural properties of synthetic and natural products due to an efficient balance between computational cost and accuracy [45]. Frontier molecular orbitals, molecular electrostatic potential (MEP) and the $E_{HOMO}$-$E_{LUMO}$ gap were also computed at the B3LYP/6-311G(d,p) level of theory.

### *2.5. Molecular Docking Method*

The graphical interface of the Chemical Computing Inc, Molecular Operating Environment (MOE) 2017 tool was used to import CIF files of the newly synthesized Complex **1** and its ligands at the MOPAC 7.0 level of theory. Geometry relaxation was performed at the same level of theory and structures were entered into the database. The X-ray crystallographic structure DNA gyrase enzyme possessing PDB (ID: 1KIJ) with a resolution of 2.30 Å was extracted from PDB [46]. The extracted 1KIJ structure was imported to the MOE GUI, protonated and optimized using the protonate-3D and minimize menu of the MOE modeling suite. Water molecules attached with 1KIJ were removed by using the sequence editor of the MOE panel. For the purpose of docking analysis, 1KIJ coordinates were relaxed using an AMBER force field and semiempirical PM3 approaches. The relaxed coordinates had minimum energy and stable conformation for the best scoring function calculations. After preparation, Complex **1** was docked with 1KIJ. To perform docking and achieve binding information of Complex **1** and its ligands with 1KIJ, the optimized structure of **1** was subjected to methodical molecular docking taking the enzyme as a receptor at default parameters with an RMS gradient of 0.01 kcal $mol^{-1}$. Site Finder was employed to find the active sites of 1KIJ. A number of docking runs were endorsed for the final docking poses to be as accurate as possible. At every step of the simulation, the interaction energy of Complex **1** and its ligands with 1KIJ was determined to calculate binding affinity. The remaining parameters were kept as a default [47].

### *2.6. Antimicrobial Test*

The wells (6 mm in diameter) were dug in the Mueller–Hinton Agar (MHA) with the help of a sterile cork borer. Single bacterial colonies were standardized in peptone broth to reach the turbidity of the McFarland 0.5 standard and the standardized bacteria inocula were spread on the surface of the MHA with the help of a sterile swab stick. Three Gram-negative bacteria (*Klebsiella pneumoniae, Acinectobacter baumannii and Pseudomonas aeruginosa*) and one Gram-positive bacterium (*Staphylococcus aureus*) of clinical origin were obtained from the Department of Microbiology Laboratory, University of Ilorin, Ilorin, Nigeria. All the microorganisms were used to test the antibacterial activity of the compounds and the results were obtained by the agar well diffusion method using a 30 mg/5 mL concentration (in DMSO) with a volume of 50 µL per well [48]. Another well was supplemented with DMSO as a negative control and antibiotic susceptibility of the bacteria was also carried out as a positive control. The plates were prepared in triplicate and incubated immediately at 37 °C for 24 h. Antibacterial activity was determined by measuring the diameter of the complete growth inhibition zone in millimeters (mm). The results are the average of three trials and are stated as average ± standard deviation.

### *2.7. Synthesis*

Synthesis of $Cu(BZDH)_2(4Clbz)_2$ (1)

To a 20 mL ethanol–water (1:1) solution of 4-chlorobenzoic acid (2 mmole, 0.313 g) and NaOH (2 mmole, 0.080 g), $Cu(NO_3)_2.3H_2O$ (2 mmol, 0.482 g) was added with continuous stirring at room temperature, followed by benzimidazole (2 mmole, 0.236 g), which was added gradually. The whole resulting solution was stirred for 2 h. The blue solution obtained was filtered and kept at room temperature, and after 3 days, blue crystals suitable for single-crystal X-ray analysis were obtained. The blue crystals were removed from the mother liquor and dried in air at room temperature. Yield, 69%, M. wt. = 610.93 g/mol, m.pt. = 230 °C, IR (KBr, $cm^{-1}$): 3138, 3115, 3053, 2916, 1624, 1595, 1498, 1465, 1421, 1385, 1352, 1321, 1304, 1275, 1249, 1196, 1153, 1113, 1034, 1011, 976, 939, 885, 850, 839, 826, 775, 764, 743, 617, 547, 439, 424.

## 3. Result and Discussion

### *3.1. Synthesis*

A new copper(II) complex of benzimidazole and 4-chlorobenzoic acid was synthesized. The complex was synthesized step-by-step at room temperature. The first step for the synthesis involved the reaction of 4-chlorobenzoic acid with NaOH. Then, copper(II) nitrate and benzimidazole were added. After a few days, some blue single crystals of the complex were obtained at room temperature through solvent evaporation. The step-by-step route for **1** is shown in Scheme 1.

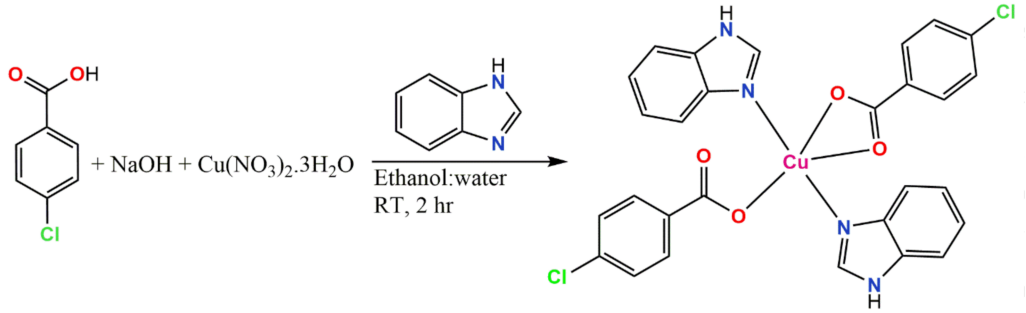


**Scheme 1.** Synthetic route for **1**.

### *3.2. Structural Description*

The mononuclear $Cu^{II}$ complex crystallized in the monoclinic system with the centrosymmetric space group $P2_1/c$. The molecular structure of **1** is shown in Figure 2. Selected bond lengths are given in Table 2. The five-coordinate Cu atom is surrounded by two trans monodentate benzimidazole ligands and two 4-chlorobenzoate anions in which one carboxylate is monodentate and the other is in a chelating bidentate mode. The bond valences around the $Cu^{II}$ ion were computed according to Brown [49] and O'Keeffe and Brese [50] as $\nu_{ij} = \exp[(R_{ij} - d_{ij})/0.37]$, where $R_{ij}$ is the bond valence parameter (in the formal sense, it is the single-bond length between the i and j atoms) and $d_{ij}$ is the observed bond length. The sum of the bond valences formed by the atom is assumed to be equal to the valence (formal oxidation state) of the atom. The $R_{Cu-O}$ and $R_{Cu-N}$ values were taken as 1.679 Å and 1.713 Å, respectively [51]. The four strong Cu–O and Cu-N equatorial bonds have bond valences ranging from 0.43 to 0.49 and the axial Cu–O2 bond of 2.440(2) Å has a bond valence of 0.13. Finally, the valence of the five-coordinate Cu atom is consistent with the valence sum rule ($V_i = \Sigma\nu_{ij}$), which gives $V_{Cu}$ = 1.95 v.u. The calculated valence of the very long contact Cu···O4 of 3.0219(19) Å is only 0.027 v.u., indicating the lack of interaction between these two atoms. The observed square pyramidal (SQP) environment of the $Cu^{II}$ complex is slightly distorted toward a trigonal—bipyramidal (TBP) coordination, with the trigonality parameter $\tau$ = 0.045 (as defined by Addison et al. [52], where $\tau$ is equal to 0 for a regular SQP structure and **1** for TBP). The N—H···O hydrogen bonds [N2-H1 ... $O4^{\#I}$ and N4-H2 ... $O4^{\#II}$] (Table 3) link the molecules into the chains extending along the crystallographic b-axis (Figure 3a), with a C(8) first-level graph-set motif [53,54]. According to the second-level graph theory, the molecules are joined in pairs of dimers to form the ring motif $R^2_2(16)$ (Figure 3b). The combined effect of the sterically hindered carboxylate ligand and the intramolecular hydrogen-bonding interactions changes the binding mode of the carboxylate ligands from bidentate to monodentate. This rather unusual environment around the central atom was previously observed in Cu, Fe and Co complexes [54–56].

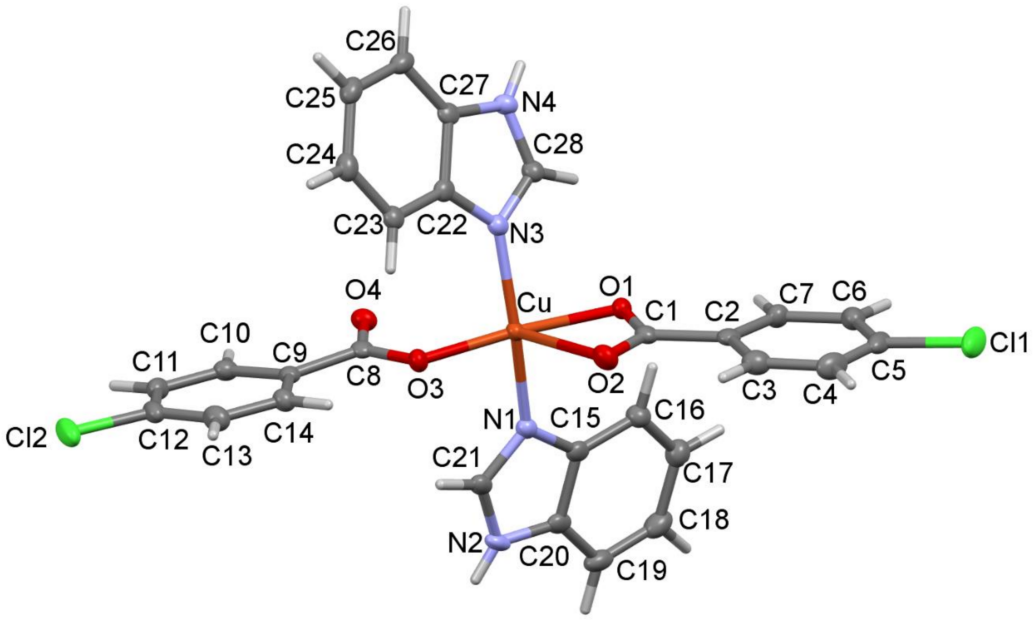


**Figure 2.** Ortep drawing of $Cu(BZDH)_2(4Clbz)_2$ (**1**) showing the 50% probability of thermal ellipsoids.

**Table 2.** Selected bond lengths (Å) and bond angles (°) for **1**.

| Atoms | 1<br>Bond Length (Å) |
|---|---|
| Cu-O1 | 1.9873(18) |
| Cu-O2 | 2.440(2) |
| Cu-O3 | 1.9406(18) |
| Cu-N1 | 2.015(2) |
| Cu-N3 | 2.004(2) |
| **Atoms** | **1<br>Bond Angle (°)** |
| O1-Cu-O2 | 58.89(7) |
| O1-Cu-O3 | 167.73(7) |
| O1-Cu-N1 | 91.40(8) |
| O1-Cu-N3 | 89.00(8) |
| O2-Cu-O3 | 108.84(7) |
| O2-Cu-N1 | 96.30(8) |
| O2-Cu-N3 | 96.85(8) |
| O3-Cu-N1 | 90.41(9) |
| O3-Cu-N3 | 92.40(8) |
| N1-Cu-N3 | 164.87(9) |

**Table 3.** Hydrogen-bonding parameters for Compound **1**.

| Compound | D–H … A | d(D–H) | d(H … A) | d(D … A) | <(DHA) |
|---|---|---|---|---|---|
| 1 | N2-H1 … $O4^{\#I}$ | 0.79(4) | 2.32(4) | 3.041(3) | 153(3) |
| | N4-H2 … $O4^{\#II}$ | 0.83(4) | 2.03(4) | 2.813(3) | 160(3) |
| | C16-H16-O1 | 0.95 | 2.32 | 2.991(3) | 128 |
| | C21-H21-$O2^{\#III}$ | 0.95 | 2.30 | 2.969(4) | 127 |

Symmetry code: (#I) 1 −.x, 1/2 + y, 3/2 − z; (#II) 1 − x, −1/2 + y, 3/2 − z, (#III) 1 − x, 1 − y, 1 − z.

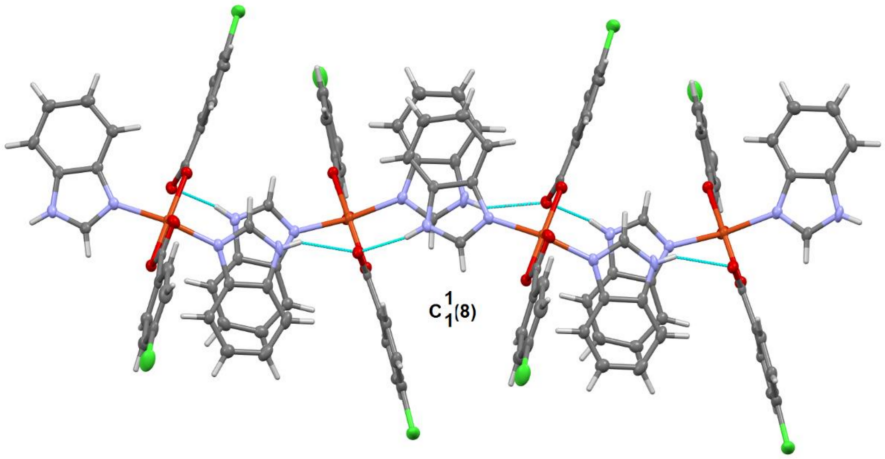


**(a)** View of the C(8) motif

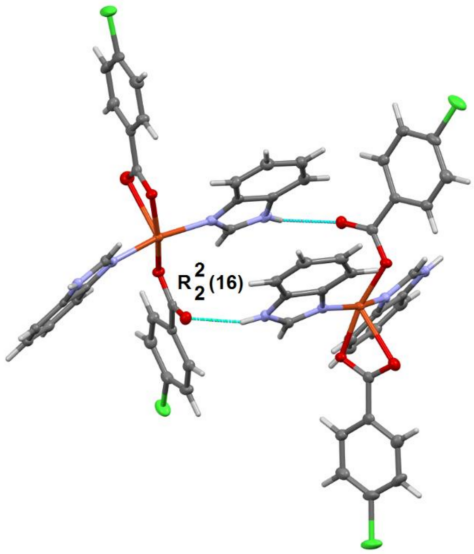


**(b)** View of the $R^2_2(16)$ motif

**Figure 3.** Structural packing motifs in **1** showing the N-H . . . O hydrogen bonds.

### *3.3. Infrared Spectra*

The infrared spectra of Complex **1** and benzimidazole were recorded in the 4000–400 $cm^{-1}$ region and are presented in Figure 4. Important assignments were discussed as follows: the absorption bands in the region 3200–2900 $cm^{-1}$ showed the presence of C-H aromatic and N-H stretching vibration of the benzoate anion and benzimidazole in Complex **1**. The stretching band of C-Cl was observed at around 743 $cm^{-1}$. The appearance of a new band in the region of 1624 $cm^{-1}$ is assigned to the C=C stretching vibration in the benzoate molecule. The absorption band at 1551–1499 $cm^{-1}$ is assigned to the v(C=N) stretching vibration. The bands observed at 1595 $cm^{-1}$ are assigned to the asymmetric vibration of the carboxylate group of chlorobenzoate and two other bands were seen on the spectra, namely 1385 and 1352 $cm^{-1}$, which are assigned to the symmetric vibration of the carboxylate group of chlorobenzoate. The differences in $V_{as}$(OCO) and $V_s$(OCO) are 210 and 242 $cm^{-1}$, which are indicative of the asymmetric bidentate mode of coordination and monodentate mode of coordination of the carboxylato groups to the center Cu(II) [57]. The peaks at 547 and 439 $cm^{-1}$ are assigned to Cu-O and Cu-N [58] for the *p*-chlorobenzoate moiety and stretching band for benzimidazole. These illustrations correspond to the crystal structure of Complex **1**.

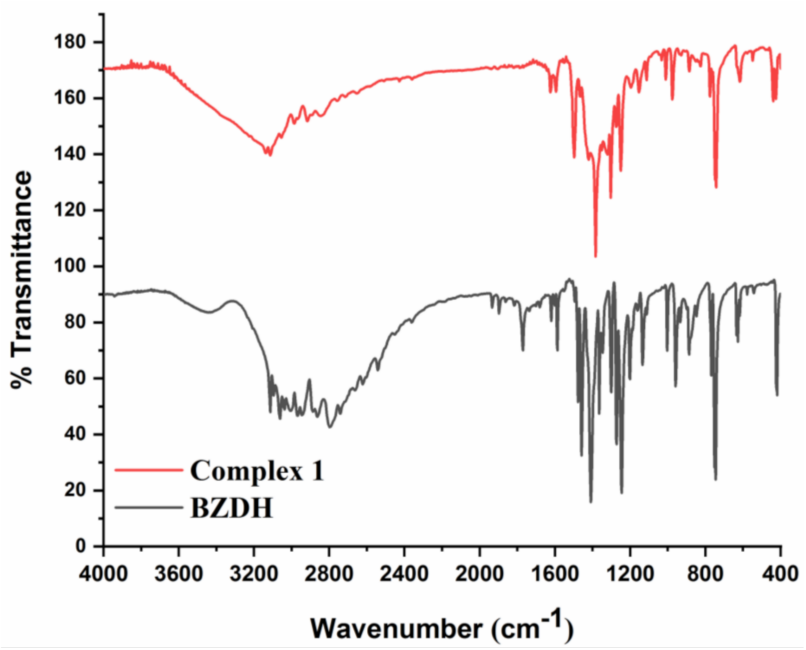


**Figure 4.** FTIR spectra of Complex **1** and benzimidazole (BZDH).

### *3.4. The UV Spectrum of the Complex*

The UV–visible spectrum of the newly synthesized Complex **1** was recorded in the DMSO solution and is shown in Figure 5. Complex **1** exhibited a broad d–d absorption at 746 nm (13405 $cm^{-1}$). The appearance of a broad absorption is attributed to the d→d electronic transition, which corresponds to those of the distorted square pyramidal geometry [52,58]. This suggests that the $CuN_2O_3$ chromophore keeps its identity in the solution state as well.

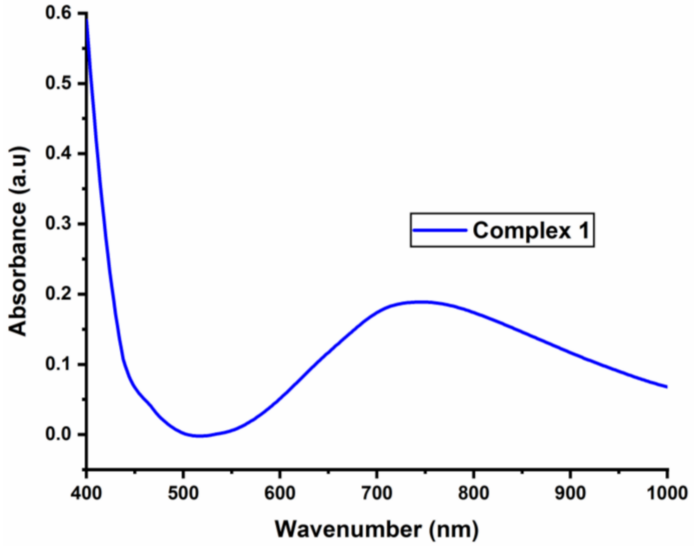


**Figure 5.** UV—vis spectrum of Complex **1.**

### *3.5. Hirschfeld Surfaces Analysis*

HS analysis was applied to compare quantitatively the different intermolecular interactions affecting the molecular packing in **1.** The analysis was performed and mapped over $d_{norm}$ in the range of -0.5854 to 1.344 Å. The red spots observed on the Hirschfeld surface are due to hydrogen bonding N—H···O interactions (Figure 6).

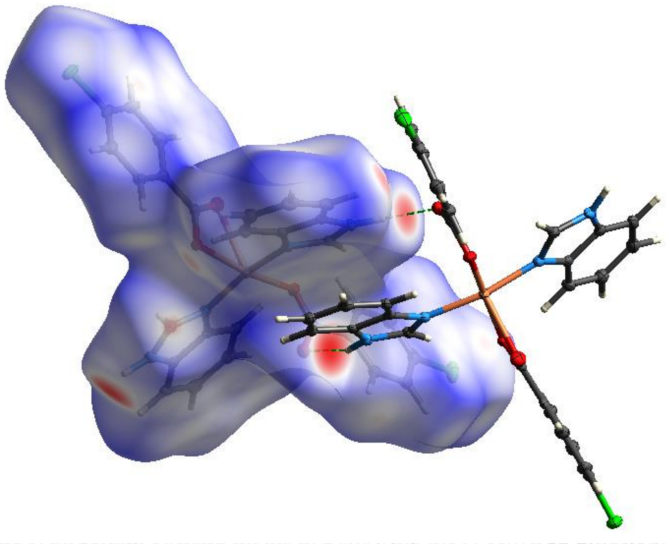

**Figure 6.** Hirschfeld surfaces (HS) of **1** mapped with $d_{norm}$.

The most significant intermolecular interactions are shown in Figure 7. The predominant interactions H . . . H (31.1%) appear in the middle of the scattered points in the fingerprint plot. The second most important interactions H . . . C (24.4%) are characterized by symmetrical wings in the FP. Interestingly, there seems to be quite a large share of H...Cl (16.4%) contacts. The sharp symmetrical spikes on FP represent H . . . O (12.7%) interactions. The C . . . C contacts (6.6%) are associated with the partial π–π stacking interactions of benzimidazole ligands.

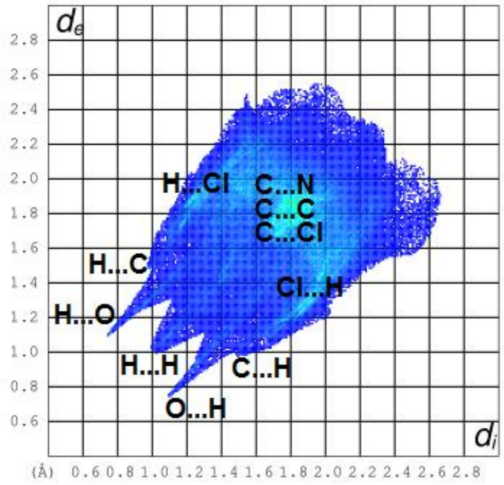


**Figure 7.** Fingerprint plot of the most significant noncovalent interactions of **1**.

The percentages of intermolecular contributions are summarized in Figure 8. The eight significant (>2%) types of interactions include H . . . H, H . . . C/C . . . H, H . . . Cl/Cl . . . H, H . . . O/O . . . H, C . . . C H . . . N/N . . . H, C . . . Cl/Cl . . . C and N . . . C/C . . . N and are listed in decreasing order.

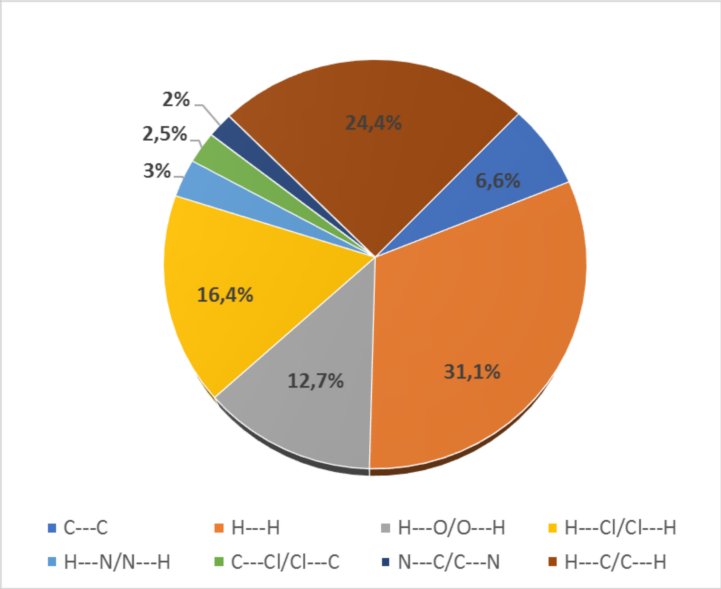


**Figure 8.** Summary of the intermolecular interactions (>2%) in **1**.

### *3.6. Structural Analysis*

Structural geometries of Complex **1** were simulated and optimized using DFT/B3LYP to find the geometric (bond lengths, bond angles) and electronic parameters ($E_{HOMO}$, $E_{LUMO}$ and MESP). Optimized geometries of Complex **1** are displayed in Figure 9, with a symmetric charge distribution on each individual atom of Complex **1**.

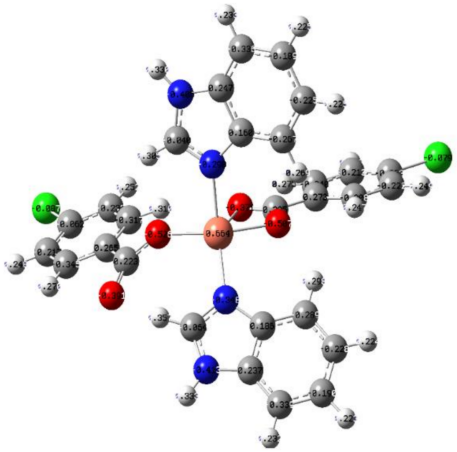

**Figure 9.** The optimized geometry of **1** at the B3LYP/6-31G (d,p) level of theory.

#### 3.6.1. Frontier Molecular Orbitals (FMOs) Analysis

The frontier molecular orbital (FMOs) calculations were performed using quantum chemistry. The DFT approach is a popular way to describe the distribution of electron densities. The corresponding $E_{HOMO}$ and $E_{LUMO}$ values were found to be −6.55 eV and −1.38 eV, respectively, for **1**. The HOMO–LUMO gap (i.e., ΔE) for **1** was found to be 5.16 eV (Figure 10). To comprehend the distribution of isodensities, HOMO and LUMO surfaces were investigated revealing most distributions of isodensities on heteroatoms.

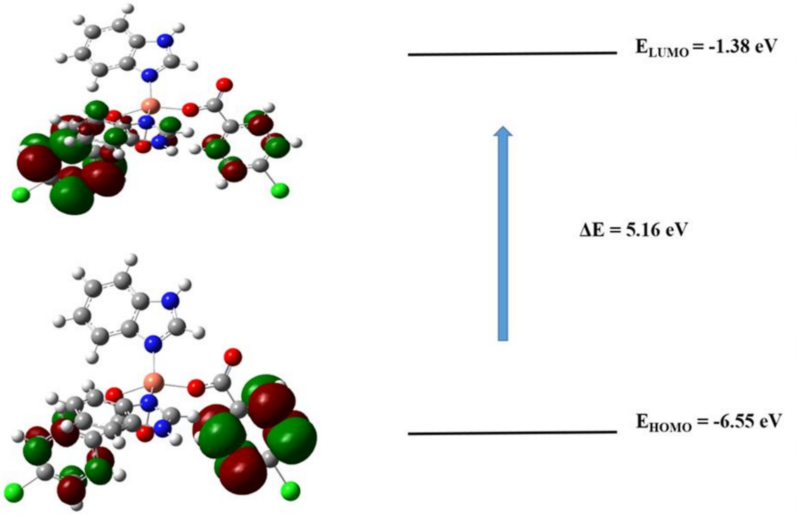


**Figure 10.** HOMO, LUMO, $E_{HOMO}$, $E_{LUMO}$ and band gap (ΔE) for **1.**

### 3.6.2. Molecular Electrostatic Potential Analysis

The optimized geometry of **1** at the B3LYP/6- 31G(d,p) level of theory was used to map the molecular electrostatic potential surfaces (MESP) and are depicted in Figure 11, which reveals that the negative potential is concentrated on the oxygen and nitrogen atoms, reflecting electron transfer from O and N (labeled with red contours). The dispersion of potential for **1** ranges from −0.237 to 0.237 esu, indicating electrophilic and nucleophilic centers in this range. The red color indicates that –O and –N centers contribute as nucleophilic regions whereas the gray color indicates that –C and –H atoms contribute as electrophilic regions.

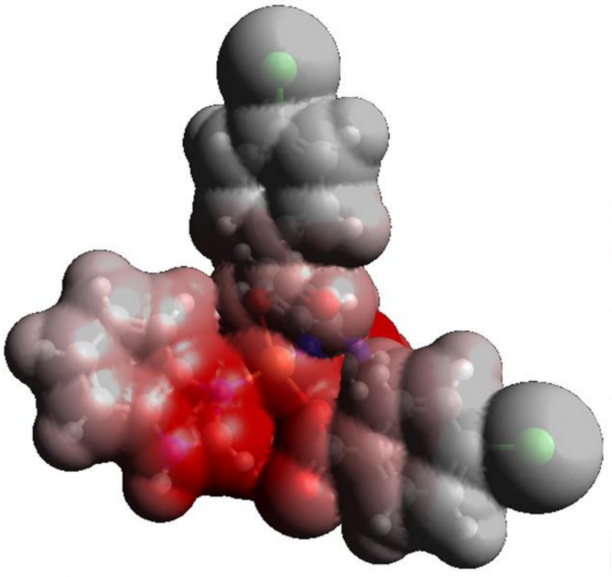

**Figure 11.** Molecular electrostatic potential surfaces (MESP) of **1** mapped at the B3LYP/6-31G (d,p) level of theory.

### 3.6.3. Reactivity Parameters

The global chemical reactivity descriptors such as ionization potential (I) [45], electron affinity (A), softness (S), hardness (η), chemical potential (μ), softness (S), electronegativity (χ) [59,60] and electrophilicity index (ω) [61,62] are determined on the basis of the HOMO and LUMO energy [63] values as shown below in [64]:

Ionization potential (I) = $-E_{HOMO}$;
Electron affinity (A) = $-E_{LUMO}$;
Chemical hardness (η) = (I − A)/2;
Chemical potential (μ) = −(I + A)/2;
Softness (S) = $\frac{1}{2}\eta$;
Electronegativity (χ) = (I + A)/2;
Electrophilicity index (ω) = $\mu^2/2\eta$.

Table 4 indicates that **1** shows some reactive potential on the basis of ionization potential. Chemical hardness η is less in **1,** which reveals significant reactivity. Complex **1** has moderate softness (S) showing its polarizable and reactive nature. The electronegativity (χ) and electrophilicity index (ω) also determined a significant increase in the reactivity of Complex **1**.

**Table 4.** Global chemical reactivity descriptors obtained from B3LYP with the basis set Lanl2dz.

| Complex | I (eV) | A (eV) | η (eV) | μ (eV) | S (eV) | χ (eV) | ω (eV) |
|---|---|---|---|---|---|---|---|
| **1** | 6.655 | 1.387 | 2.633 | −4.0214 | 0.18985 | 4.02140 | 3.07026 |

### *3.7. Molecular Docking Studies*

In an attempt to comprehend the enzyme inhibition activity of the newly synthesized Complex **1** and its ligands, the molecular docking approach was employed to determine the strength of interactions and binding modes. Pose view analysis and conformations of Complex **1** and its ligands with the lowest free energy are depicted in Figure 12a–c for the DNA gyrase enzyme. It is revealed that **1** is the most potent compared to its ligands due to having the highest negative free energy value (26.31 $kJmol^{-1}$), evident in Table 5. Docked Complex **1** and its ligands with 1KIJ were analyzed for various types of interactions such as hydrogen bonding, hydrophobic and van der Waals interactions. These interactions express the ability to block the active sites of 1KIJ. The 2D ligplot indicates that the high binding affinity of Complex **1** compared to its ligands are attributed to its greater interactions with residues of 1KIJ which furnishes three electrostatic interactions. The ligplot in Figure 12a indicates that the $N^+$ of Complex **1** develops electrostatic interactions with the negatively charged –O of the asparagine Asn(95) residue of 1KIJ, whereas the negatively charged carbene of **1** also develops electrostatic interactions with the positively charged −H of lysine Lys(87). Another interaction is between the positively charged $N^+$ of **1** and negatively charged O of glutamic acid Glu(85). On the other hand, organic ligands of **1** only develop hydrophobic interactions with the core of the enzyme pocket leading to their lower binding affinity compared to Complex **1** (Figure 12a,c).

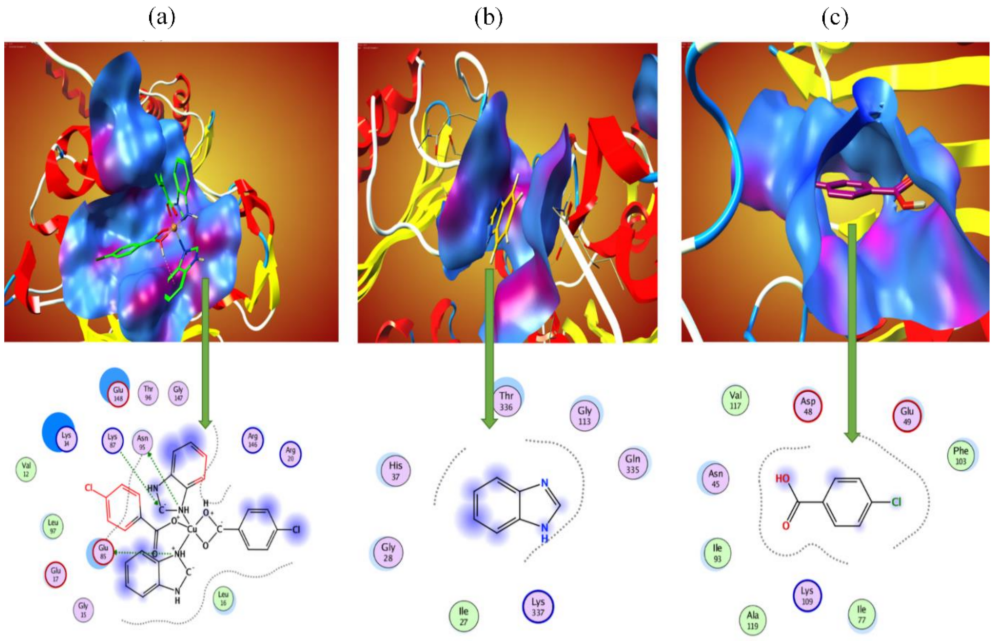


**Figure 12.** Molecular docked complexes of (**a**) Complex 1, (**b**) benzimidazole and (**c**) 4-chlorobenzoic acid with the DNA gyrase enzyme (top line). The bottom line shows ligplots of the respective complex and its organic ligands with residues of the DNA gyrase enzyme calculated at the PM3 semiempirical level of theory.

**Table 5.** Binding constants and free energy values for the interaction of the A2 complex and its ligands with DNA gyrase calculated from the molecular docking data.

| Complexes | Molecular Docking | |
|---|---|---|
| | "$K_b$"/$M^{-1}$ | ΔG/KJmol$^{-1}$ |
| Complex **1** | $4.09 \times 10^4$ | −26.31 |
| Benzimidazole | $9.54 \times 10^2$ | −17.00 |
| 4-Chlorobenzoic acid | $1.94 \times 10^3$ | −18.75 |

### *3.8. Antibacterial Test*

The solvent used (DMSO), benzimidazole (BZDH) and $Cu(BZDH)_2(4Clbz)_2$ (**1**) were tested on three Gram-negative bacteria (*Klebsiella pneumoniae, Acinectobacter baumannii* (G-) and *Pseudomonas aeruginosa)* and one Gram-positive (G+) bacterium (*Staphylococcus aureus*). Investigation of the antibacterial activity was carried out by using the agar well diffusion method where each well contained a 50 µL of a 30 mg/5 mL concentration of the compounds. The summary of the results is given in Table 6 where cefuroxime, gentamicin, ceftazidime, ofloxacin, amoxicillin/clavulanate, nitrofurantoin, ampicillin and ciprofloxacin were used as the positive control for both G- and G+ while DMSO was used as the negative control in the experiment. The parent ligand, benzimidazole, shows antibacterial activity against *Staphylococcus aureus* and *Acinectobacter baumannii* with inhibition zones of 12.2 ± 1.3 and 9.5 ± 1.1 mm, respectively. Benzimidazole shows no activity for both *K. pneumoniae and P. aeruginosa.* Compound **1** showed a strong antibacterial effect against three (3) bacterial strains, namely *S. aureus, A. baumannii* and *P. aeruginosa* with inhibition zones measured at 20.4 ± 0.8, 11.0 ± 1.2 and 17.3 ± 0.3 mm, respectively, whereas no activity was found in *K. pneumoniae*. The activity against *S. aureus* and *P. aeruginosa* is very notable in **1** compared to the parent ligand. From the results (Table 6), it can be deduced that Compound **1** is more effective and possesses higher efficacy in antibacterial testing compared to the parent ligand and some of the standard antibiotic drugs used in the current work. Compound **1** was able to depopulate some of the microorganism strains that were used more

compared to benzimidazole. Upon complexation, the antibacterial effect increases, which reduces the survival rate of the strains. Copper(II) is known to be a bacterial killer because of its ability to interact with lipids, making holes in the cell membranes and leaking out of required solutes for the survival of the cell [65]. It is also established that chelation can reduce the polarity of the metal ion through partial sharing of its positive charge with the donor group of the active compounds [66]. Coordination enhances the lipophilic character of the metal ion and the permeation of the metal ions through the lipid layers of cellular membrane increases, obstructing the growth of bacteria [66].

**Table 6.** Antibacterial activity of selected compounds.

| Test Organisms Compounds | Inhibition Zone Diameter (mm) (± Standard Deviation) Data Are Stated as Average Standard Deviation (N = 3) | | | |
|---|---|---|---|---|
| | *S. aureus* (G−) | *K. pneumoniae* (G+) | *A. baumannii* (G+) | *P. aeruginosa* (G+) |
| BZDH | 12.2 ± 1.3 | 0 | 9.5 ± 1.1 | 0 |
| **1** | 20.4 ± 0.8 | 0 | 11.0 ± 1.2 | 17.3 ± 0.3 |
| Ofloxacin | 18.2 ± 0.9 | 0 | 18.0 ± 1.3 | 0 |
| Amoxicillin/Clavulanate | 0 | 0 | 20.6 ± 1.2 | 0 |
| Ceftazidime | 0 | 0 | 14.3 ± 1.2 | 0 |
| Cefuroxime | 0 | 0 | 14.1 ± 0.2 | 0 |
| Gentamicin | 12.0 ± 1.1 | 16.3 ± 1.2 | 18.5 ± 0.6 | 11 ± 0.9 |
| Nitrofurantoin | NA | 25.1 ± 0.2 | 23.2 ± 1.1 | 0 |
| Ciprofloxacin | NA | 18.3 ± 0.7 | 20.7 ± 1.1 | 0 |
| Ampicillin | NA | 0 | 16.5 ± 0.4 | 0 |

All microorganisms were resistant to DMSO. The concentration was 30 mg/5 mL in DMSO. Zero (0) indicates no inhibition.

## 4. Conclusions

In this report, a new mononuclear $Cu^{II}$ carboxylate complex was synthesized via the reaction of hydrated copper nitrate, *p*-chlorobenzoic acid (4Clbz), in the presence of benzimidazole. Subsequently, the obtained compound was characterized by single-crystal X-ray diffraction analysis, FTIR and UV–vis spectroscopy. Complex **1** is structurally interesting, owing to the asymmetrical coordination of carboxylic anions to the $Cu^{II}$ center. Optimization of the structure was carried out at the DFT/B3LYP level. Complex **1** showed a higher microbial killing rate against Gram-positive and Gram-negative bacteria compared to benzimidazole. The results obtained from the computational molecular docking studies of **1** show a higher binding strength and greater interactions compared to its organic parent ligands. The docking results also validate the high potency of Complex **1** in comparison with the free benzimidazole in the antibacterial studies.

**Author Contributions:** A.A.A.; Conceptualization, methodology, investigation, writing—original draft, writing—review and editing, F.P.; formal analysis, visualization, software, writing—original draft, K.J.; visualization, I.I.A.; investigation, S.E.S.; investigation, L.S.; formal analysis, investigation, visualization, W.M.; formal analysis, investigation, visualization, software, writing—original draft, writing—review and editing. All authors have read and agree to the published version of the manuscript.

**Funding:** This research received no external funding.

**Acknowledgments:** The authors gratefully acknowledge their departments, institute and organization for this collaborative research work.

**Conflicts of Interest:** The authors declare no conflict of interest.

## References


1. Rafique, S.; Idrees, M.; Nasim, A.; Akbar, A.; Athar, A. Transition metal complexes as potential therapeutic agents. *Biotechnol. Mol. Biol. Rev.* **2010**, *5*, 38–45. [CrossRef]
2. Schatzschneider, U. Photoactivated Biological Activity of Transition-Metal Complexes. *Eur. J. Inorg. Chem.* **2010**, *2010*, 1451–1467. [CrossRef]
3. Frei, A. Metal Complexes, an Untapped Source of Antibiotic Potential? *Antibiotics* **2020**, *9*, 90. [CrossRef] [PubMed]
4. Iakovidis, I.; Delimaris, I.; Piperakis, S.M. Copper and Its Complexes in Medicine: A Biochemical Approach. *Mol. Biol. Int.* **2011**, *2011*, 1–13. [CrossRef] [PubMed]
5. Duncan, C.; White, A.R. Copper complexes as therapeutic agents. *Metallomics* **2012**, *4*, 127–138. [CrossRef]
6. Zhang, C.X.; Lippard, S.J. New metal complexes as potential therapeutics. *Curr. Opin. Chem. Biol.* **2003**, *7*, 481–489. [CrossRef]
7. Obaleye, J.A.; Ajibola, A.A.; Bernardus, V.B.; Hosten, E.C. Synthesis, X-ray crystallography, spectroscopic and in vitro antimicrobial studies of a new Cu(II) complex of trichloroacetic acid and imidazole. *J. Mol. Struct.* **2020**, *1203*, 127435. [CrossRef]
8. Baldini, M.; Belicchi-Ferrari, M.; Bisceglie, F.; Dall'Aglio, P.P.; Pelosi, G.; Pinelli, S.; Tarasconi, P. Copper(II) Complexes with Substituted Thiosemicarbazones of α-Ketoglutaric Acid: Synthesis, X-ray Structures, DNA Binding Studies, and Nuclease and Biological Activity. *Inorg. Chem.* **2004**, *43*, 7170–7179. [CrossRef]
9. Efthimiadou, E.K.; Katsaros, N.; Karaliota, A.; Psomas, G. Mononuclear copper(II) complexes with quinolones and nitrogen-donor heterocyclic ligands: Synthesis, characterization, biological activity and interaction with DNA. *Inorg. Chim. Acta* **2007**, *360*, 4093–4102. [CrossRef]
10. Renfrew, A.K. Transition metal complexes with bioactive ligands: Mechanisms for selective ligand release and applications for drug delivery. *Metallomics* **2014**, *6*, 1324–1335. [CrossRef]
11. Li, H.; Yin, K.-L.; Xu, D.-J. catena-Poly[[bis(1H-benzimidazole-κ$N^3$)(salicylato-κO)copper(II)]-μ-salicylato-O,O′:O′′]. *Acta Cryst.* **2005**, *C61*, m19–m21. [CrossRef] [PubMed]
12. Bansal, Y.; Silakari, O. The therapeutic journey of benzimidazoles: A review. *Bioorganic Med. Chem.* **2012**, *20*, 6208–6236. [CrossRef] [PubMed]
13. Gurer-Orhan, H.; Orhan, H.; Suzen, S.; Püsküllü, M.O.; Buyukbingol, E. Synthesis and evaluation of in vitro antioxidant capacities of some benzimidazole derivatives. *J. Enzym. Inhib. Med. Chem.* **2006**, *21*, 241–247. [CrossRef] [PubMed]
14. Spasov, A.A.; Yozhitsa, I.N.; Bugaeva, L.I.; Anisimova, V.A. Benzimidazole derivatives: Spectrum of pharmacological activity and toxicological properties (a review). *Pharm. Chem. J.* **1999**, *33*, 232–243. [CrossRef]
15. Matejová, S.; Puchoňová, M.; Mazúr, M.; Valigura, D.; Rohlíček, J.; Jorík, V.; Moncoľ, J. Preparation, spectral properties and structure of bis(salicylato)bis(benzimidazole)-copper(II) complexes with two different benzimidazole spatial orientation. *Polyhedron* **2019**, *170*, 86–94. [CrossRef]
16. Yoe, F.; Flores-Álamo, M.; Morales, F.; Escudero, R.; Cortes-Hernández, H.; Castro, M.; Barba-Behrens, N. Structural, magnetic and theoretical study of mononuclear nickel(II) and cobalt(II) compounds of a benzimidazole thiobutanoic acid derivative. *Inorg. Chim. Acta* **2014**, *423*, 36–45. [CrossRef]
17. Huang, X.; Xiao, L.-P.; Xu, D.-J. Bis(benzimidazole-κN)bis(3,5-dihydroxybenzoato-κO)copper(II) trihydrate. *Acta Crystallogr. Sect. E Struct. Rep. Online* **2006**, *62*, 5. [CrossRef]
18. Devereux, M.; O'Shea, D.; O'Connor, M.; Grehan, H.; Connor, G.; McCann, M.; Rosair, G.M.; Lyng, F.M.; Kellett, A.; Walsh, M.; et al. Synthesis, catalase, superoxide dismutase and antitumour activities of copper(II) carboxylate complexes incorporating benzimidazole, 1,10-phenanthroline and bipyridine ligands: X-ray crystal structures of $[Cu(BZA)_2(bipy)(H_2O)]$, $[Cu(SalH)_2(BZDH)_2]$ and $[Cu(CH_3COO)_2(5,6\text{-DMBZDH})_2]$ ($SalH_2$ = salicylic acid; BZAH = benzoic acid; BZDH = benzimidazole and 5,6-DMBZDH = 5,6-dimethylbenzimidazole). *Polyhedron* **2007**, *26*, 4073–4084. [CrossRef]
19. Su, J.-R.; Gu, J.-M.; Xu, D.-J. Bis(1*H*-benzimidazole-κ$N^3$)bis(4-hydroxybenzoato-κ$^2$O,O′)copper(II). *Acta Crystallogr. Sect. E Struct. Rep. Online* **2005**, *61*, 244. [CrossRef]
20. Yıldırım, M.H.; Heren, Z.; Paşaoğlu, H.; Hıra, D.; Buyukgungor, O. Bis-(benzimidazole-κN)bis(2-benzoyl-benzoato-κO)copper(II). *Acta Crystallogr. Sect. E Struct. Rep. Online* **2009**, *65*, m638–m639. [CrossRef]

21. Puchoňová, M.; Švorec, J.; Švorc, Ľ.; Pavlik, J.; Mazúr, M.; Dlháň, Ľ.; Růžičková, Z.; Moncol, J.; Valigura, D. Synthesis, spectral, magnetic properties, electrochemical evaluation and SOD mimetic activity of four mixed-ligand Cu(II) complexes. *Inorg. Chim. Acta* **2017**, *455*, 298–306. [CrossRef]
22. Song, W.-D.; Huang, X.-H.; Wang, H. Bis(1H-benzimidazole-κN)bis-(4-methyl-benzoato-κO,O′)copper(II). *Acta Crystallogr. Sect. E Struct. Rep. Online* **2008**, *64*, m764. [CrossRef] [PubMed]
23. O'Connor, M.; Kellett, A.; McCann, M.; Rosair, G.; McNamara, M.; Howe, O.; Creaven, B.S.; McClean, S.; Kia, A.F.-A.; O'Shea, D.; et al. Copper(II) Complexes of Salicylic Acid Combining Superoxide Dismutase Mimetic Properties with DNA Binding and Cleaving Capabilities Display Promising Chemotherapeutic Potential with Fast Acting in Vitro Cytotoxicity against Cisplatin Sensitive and Resistant Cancer Cell Lines. *J. Med. Chem.* **2012**, *55*, 1957–1968. [CrossRef]
24. Wang, Y.; Shi, Q.; Yang, B.; Shi, Q.; Gao, Y.; Zhou, Z. Synthesis, crystal structure and forming mechanism of two novel copper (II) α-methacrylate complexes with benzimidazole. *Sci. China Ser. B Chem.* **1999**, *42*, 363–372. [CrossRef]
25. Obaleye, J.A.; Ajibola, A.A.; Bernardus, V.B.; Hosten, E.C.; Ozarowski, A. Synthesis, spectroscopic, structural and antimicrobial studies of a dimeric complex of copper(II) with trichloroacetic acid and metronidazole. *Inorg. Chim. Acta* **2020**, *503*, 119404. [CrossRef]
26. Chakraborty, I.; Pinto, M.; Stenger-Smith, J.; Martinez-Gonzalez, J.; Mascharak, P.K. Synthesis, structures and antibacterial properties of Cu(II) and Ag(I) complexes derived from 2,6-bis(benzothiazole)-pyridine. *Polyhedron* **2019**, *172*, 1–7. [CrossRef]
27. Festa, R.A.; Thiele, D.J. Copper: An essential metal in biology. *Curr. Biol.* **2011**, *21*, R877–R883. [CrossRef]
28. Yeşilel, O.Z.; Ilker, I.; Soylu, M.S.; Darcan, C.; Süzen, Y. Synthesis, crystal structures and antimicrobial properties of copper(II)-thiophene-2,5-dicarboxylate complexes with N-donor ligands. *Polyhedron* **2012**, *39*, 14–24. [CrossRef]
29. Yenikaya, C.; Poyraz, M.; Sarı, M.; Demirci, F.; Ilkimen, H.; Büyükgüngör, O.; Sarı, M. Synthesis, characterization and biological evaluation of a novel Cu(II) complex with the mixed ligands 2,6-pyridinedicarboxylic acid and 2-aminopyridine. *Polyhedron* **2009**, *28*, 3526–3532. [CrossRef]
30. Carter, K.P.; Zulato, C.H.F.; Cahill, C. Exploring supramolecular assembly and luminescent behavior in a series of RE-p-chlorobenzoic acid-1,10-phenanthroline complexes. *CrystEngComm* **2014**, *16*, 10189–10202. [CrossRef]
31. Carter, K.P.; Pope, S.J.A.; Cahill, C.L. A series of Ln-p-chlorobenzoic acid–terpyridine complexes: Lanthanide contraction effects, supramolecular interactions and luminescent behavior. *CrystEngComm* **2014**, *16*, 1873–1884. [CrossRef]
32. Khosravi, I.; Mirzaei, M.; Bauzá, A.; Frontera, A.; Eftekhar, M. A new oxo centered basic p-chlorobenzoate bridging heterotrinuclear complex, $[Cr_2MnO(C_7H_4O_2Cl)_6(Py)_3]C_7H_5O_2Cl$: Synthesis, X-ray crystal structure and theoretical DFT study. *Polyhedron* **2014**, *81*, 349–355. [CrossRef]
33. Abdullah, N.; Sharmin, N.; Ozair, L.N.; Nordin, A.R.; Nasir, W.S.N.M.; Mohamadin, M.I. Structures and mesomorphism of complexes of tetrakis(4-chlorobenzoate-μ-O,O′)bis(ethanol)dicopper(II) with different N-donor ligands. *J. Co-Ord. Chem.* **2015**, *68*, 1347–1360. [CrossRef]
34. Sundberg, M.R.; Uggla, R.; Kivekäs, R. Conformational isomerism and effect of complexation on carboxylate group in two crystallographically independent coordination units of trans-di(4-chlorobenzoato-O)bis(1,3-diaminopropane-N,N′)cobalt(III) 4-chlorobenzoate dihydrate. *Inorg. Chim. Acta* **1995**, *232*, 1–8. [CrossRef]
35. Köse, D.A.; Gökçe, G.; Gökçe, S.; Uzun, I. bis(N,N-diethylnicotinamide) p-chlorobenzoate complexes of Ni(II), Zn(II) and Cd(II). *J. Therm. Anal. Calorim.* **2008**, *95*, 247–251. [CrossRef]
36. *CrysAlis PRO*, version 40; Rigaku Oxford Diffraction Ltd.: Yarnton, UK, 2019.
37. Sheldrick, G.M. SHELXT—Integrated space-group and crystal-structure determination. *Acta Crystallogr. Sect. A Found. Adv.* **2015**, *71*, 3–8. [CrossRef]
38. Sheldrick, G.M. Crystal structure refinement with SHELXL. *Acta Crystallogr. Sect. C Struct. Chem.* **2015**, *C71*, 3–8. [CrossRef] [PubMed]
39. Spackman, M.A.; Jayatilaka, D. Hirshfeld surface analysis. *CrystEngComm* **2009**, *11*, 19–32. [CrossRef]
40. Spackman, M.A.; McKinnon, J.J. Fingerprinting intermolecular interactions in molecular crystals. *CrystEngComm* **2002**, *4*, 378–392. [CrossRef]
41. *CrystalExplorer*, version 17.5; University of Western Australia: Perth, Australia, 2017.

42. McKinnon, J.J.; Spackman, M.A.; Mitchell, A.S. Novel tools for visualizing and exploring intermolecular interactions in molecular crystals. *Acta Crystallogr. Sect. B Struct. Sci.* **2004**, *60*, 627–668. [CrossRef] [PubMed]
43. *Gaussian*, version 0, revision C.01; Gaussian Inc.: Wallingford, CT, USA, 2010.
44. *GaussView*, version 05; Semichem Inc.: Shawnee, OK, USA, 2009.
45. Ahmed, M.N.; Yasin, K.A.; Ayub, K.; Mahmood, T.; Tahir, M.N.; Khan, B.A.; Hafeez, M.; Ahmed, M.; Haq, I.U. Click one pot synthesis, spectral analyses, crystal structures, DFT studies and brine shrimp cytotoxicity assay of two newly synthesized 1,4,5-trisubstituted 1,2,3-triazoles. *J. Mol. Struct.* **2016**, *1106*, 430–439. [CrossRef]
46. Available online: https://www.rcsb.org/structure/1KIJ (accessed on 5 September 2020).
47. Perveen, F.; Arshad, N.; Qureshi, R.; Nowsherwan, J.; Sultan, A.; Nosheen, B.; Rafique, H. Electrochemical, spectroscopic and theoretical monitoring of anthracyclines' interactions with DNA and ascorbic acid by adopting two routes: Cancer cell line studies. *PLoS ONE* **2018**, *13*, e0205764. [CrossRef] [PubMed]
48. Abu Ali, H.; Omar, S.N.; Darawsheh, M.D.; Fares, H. Synthesis, characterization and antimicrobial activity of zinc(II) ibuprofen complexes with nitrogen-based ligands. *J. Co-Ord. Chem.* **2016**, *69*, 1110–1122. [CrossRef]
49. Brown, I.D. Bond-Length—Bond-Valence Relationships in Inorganic Solids. In *Structure Correlation*; Wiley: New York, NY, USA, 1994; pp. 405–429.
50. O'Keefe, M.; Brese, N.E. Atom sizes and bond lengths in molecules and crystals. *J. Am. Chem. Soc.* **1991**, *113*, 3226–3229. [CrossRef]
51. Sieroń, L.; Bukowska-Strzyzewska, M. catena-Poly[[bis(benzimidazole-$N^3$)copper(II)]-μ-suberato-O,O′:O″,O‴] andcatena-poly[[[bis(benzimidazole-$N^3$)copper(II)]-μ-sebacato-O,O′:O″,O‴] dihydrate]. *Acta Crystallogr. Sect. C Cryst. Struct. Commun.* **1999**, *55*, 1230–1234. [CrossRef]
52. Addison, A.W.; Rao, T.N.; Reedijk, J.; Van Rijn, J.; Verschoor, G.C. Synthesis, structure, and spectroscopic properties of copper(II) compounds containing nitrogen–sulphur donor ligands; the crystal and molecular structure of aqua[1,7-bis(N-methylbenzimidazol-2′-yl)-2,6-dithiaheptane]copper(II) perchlorate. *J. Chem. Soc. Dalton Trans.* **1984**, 1349–1356. [CrossRef]
53. Etter, M.C.; Macdonald, J.C.; Bernstein, J. Graph-set analysis of hydrogen-bond patterns in organic crystals. *Acta Crystallogr. Sect. B Struct. Sci.* **1990**, *46*, 256–262. [CrossRef]
54. Bernstein, J.; Davis, R.E.; Shimoni, L.; Chang, N.-L. Patterns in Hydrogen Bonding: Functionality and Graph Set Analysis in Crystals. *Angew. Chem. Int. Ed.* **1995**, *34*, 1555–1573. [CrossRef]
55. Kannan, S.; Venkatachalam, G.; Lee, H.-J.; Min, B.K.; Kim, W.; Koo, E.; Do, Y.R.; Yoon, S. Mononuclear transition metal complexes with sterically hindered carboxylate ligands: Synthesis, structural and spectral properties. *Polyhedron* **2011**, *30*, 340–346. [CrossRef]
56. Yoon, S.; Lippard, S.J. Synthesis and Characterization of Carboxylate-Rich Complexes Having the $\{Fe_2(\mu\text{-}OH)_2(\mu\text{-}O_2CR)\}^{3+}$ and $\{Fe_2(\mu\text{-}O)(\mu\text{-}O_2CR)\}^{3+}$ Cores of $O_2$-Dependent Diiron Enzymes. *J. Am. Chem. Soc.* **2004**, *126*, 2666–2667. [CrossRef]
57. Ross, K.A.; Dyreson, C.E.; Skiadopoulos, S.; Sirangelo, C.; Larsgaard, M.L.; Kifer, D.; Deutsch, A.; Nash, A.; Dyreson, C.; Mitra, P.; et al. ||-Coords. *Encycl. Database Syst.* **2009**, *33*, 496. [CrossRef]
58. Vicente, M.; Bastida, R.; Macıas, A.; Valencia, L.; Geraldes, C.F.G.C.; Brondino, C.D. Copper complexes with new oxaaza-pendant-armed macrocyclic ligands: X-ray crystal structure of a macrocyclic copper(II) complex. *Inorg. Chim. Acta* **2005**, *358*, 1141–1150. [CrossRef]
59. Lee, H.M.; Nolan, S.P. Efficient Cross-Coupling Reactions of Aryl Chlorides and Bromides with Phenyl- or Vinyltrimethoxysilane Mediated by a Palladium/Imidazolium Chloride System. *Org. Lett.* **2000**, *2*, 2053–2055. [CrossRef] [PubMed]
60. Polshettiwar, V.; Molnár, Á. Silica-supported Pd catalysts for Heck coupling reactions. *Tetrahedron* **2007**, *63*, 6949–6976. [CrossRef]
61. Senthilkumar, K.; Kolandaivel, P. Structure, conformation and NMR studies on 1,2-dioxane and halogen substituted 1,2-dioxane molecules. *Comput. Biol. Chem.* **2003**, *27*, 173–183. [CrossRef]
62. Arab, A.; Habibzadeh, M. Comparative hydrogen adsorption on the pure Al and mixed Al–Si nano clusters: A first principle DFT study. *Comput. Theor. Chem.* **2015**, *1068*, 52–56. [CrossRef]
63. Zgou, H.; Boussaidi, S.; Eddiouane, A.; Chaib, H.; Tripathi, R.; Ben Hadda, T.; Bouachrine, M.; Hamidi, M. New low band-gap conjugated organic materials based on fluorene, thiophene and phenylene for photovoltaic applications: Theoretical study. *Mater. Today: Proc.* **2016**, *3*, 2578–2586. [CrossRef]
64. Parr, R.G.; Szentpály, L.V.; Liu, S. Electrophilicity Index. *J. Am. Chem. Soc.* **1999**, *121*, 1922–1924. [CrossRef]

65. Chandraleka, S.; Ramya, K.; Chandramohan, G.; Dhanasekaran, D.; Priyadharshini, A.; Panneerselvam, A. Antimicrobial mechanism of copper (II) 1,10-phenanthroline and 2,2′-bipyridyl complex on bacterial and fungal pathogens. *J. Saudi Chem. Soc.* **2014**, *18*, 953–962. [CrossRef]
66. Neelakantan, M.A.; Esakkiammal, M.; Mariappan, S.S.; Dharmaraja, J.; Jeyakumar, T. Synthesis, Characterization and Biocidal Activities of Some Schiff Base Metal Complexes. *Indian J. Pharm. Sci.* **2010**, *72*, 216–222. [CrossRef]